Optimization design of slotted-interdigitated channel for stamped thin metal bipolar plate in proton exchange membrane fuel cell

Peng Hu, Linfa Peng, Weigang Zhang, Xinmin Lai*

State Key Laboratory of Mechanical System and Vibration, Shanghai Jiao Tong University, Shanghai 200240, China

ABSTRACT

The stamped metal bipolar plate is a promising candidate of the traditional graphite plate for proton exchange membrane fuel cells (PEMFCs) due to its advantages, such as low cost, compactness, robustness and high production efficiency. This study proposes a new type of flow configuration, which is called slotted-interdigitated channel, for stamped metal bipolar plates. Numerical simulation of the flow distribution of slotted-interdigitated channels is studied by using three-dimensional computational fluid dynamics (CFD) and the results show the flow distribution is uneven. Consequently, an optimization model, based on a linear analytical model, is proposed to eliminate flow maldistribution. Finally, even flow distribution is obtained according to the optimum results and high fuel cell performance can be achieved.

© 2008 Elsevier B.V. All rights reserved.

1. Introduction

Bipolar plate is one of the key components in proton exchange membrane fuel cell (PEMFC) stacks. It performs a number of essential functions in stack operation, such as reactants supply to the cell active area, current collection, and mechanical support to the membrane electrode assembly (MEA), water management, heat management and maintaining the reactants separate [1]. Two types of bipolar plates, using graphite and metal in terms of material, are commercially available [2]. Bipolar plates made of graphite are more popular currently, which have advantages including high chemical stability and high electrical conductivity. In order to reduce the size of a PEMFC stack or increase power density, the use of thin bipolar plates is essential. However, thin carbon-based bipolar plates cannot be used due to their low toughness and gas permeability. Moreover, it is difficult to manufacture the thin graphite plates.

Metal Bipolar plate is an alternative to conventional graphite bipolar plate because of its high electric conductivity in bulk, high mechanical strength, high gas impermeability, lightness. Moreover, metal bipolar plate is easy to be formed to desired shape to accommodate the flow channels using stamping method [3].

Many designs of flow configurations, for example, serpentine, parallel, discontinuous and interdigitated channel (Fig. 1), are currently used for graphite bipolar plate. But most of these designs

are not suitable for stamped metal bipolar plate. In the past few years, some studies about thin metal bipolar plate design have been reported [4–7]. There is a noticeable difference between machined graphite bipolar plate design and stamped thin metal bipolar plate design. To eliminate the need for a separate cooling plate, decrease material usage for stack construction, a continuous cooling flow field should be provided at the opposite side of the plate. That is to say, a bipolar plate is comprised with only two metal sheets which are connected together by welding, adhesion or other methods. The cooling flow field is provided between the two metal sheets and reactant gas flow fields are provided on the two outside surfaces of the sheets. For graphite bipolar plates, two irrelative flow configurations can be obtained in two sides of a single plate, respectively, using machining or chemical etching methods. However, for thin metal bipolar plate manufactured by stamping process, the flow configuration of one side of the plate is determined with the configuration of the opposite side determined. Therefore, it is difficult to obtain two continuous channels at each side on a single plate to provide reactant and cooling flow field, respectively. For example, if serpentine configuration is used (Fig. 1(A)), the reactants flow field is continuous (white colored), while the flow field on the opposite side is not continuous (dark colored). There is an exception, interdigitated channel, which can be directly used for thin metal bipolar plate. The interdigitated flow field is different from the conventional flow field in which the interdigitated flow field is not continuous (Fig. 1(D)), and the reactant gas in the fuel channel is forced to flow through diffuser and catalyst layers. For a stamped interdigitated plate, the opposite side is formed as a single serpentine configuration which can be used as cooling flow field.

---

* Corresponding author. Tel.: +86 21 34206303; fax: +86 21 62932125/103.
  E-mail address: xmlai@sjtu.edu.cn (X. Lai).

Nomenclature

A_c	cross-sectional area of channel
A_h	cross-sectional area of header
A_i	cross-sectional area of the ith channel
b_c	depth of channel
D_c	hydraulic diameter of channel
f	friction factor
F	non-uniformity index
L_c	length of channel
n	number of channels
p_{in}	pressure at inlet
p_{out}	pressure at outlet
p_c	cross-sectional perimeter of channel
R	resistance
Re	Reynolds number
$\bar{v}$	mean velocity
V_{in}	inlet velocity of the plate
w_c	width of channel

Greek letters

α	channel aspect ratio
μ	viscosity
ρ	mass density
τ_w	wall shear stress

Previous studies have shown that interdigitated flow channel reduces the possibility of flooding of the cathode electrode resulting in improved efficiency of the fuel cell, however, at the cost of a higher-pressure drop [8–13]. In the present study, a new type of flow field, slotted-interdigitated channel, based on interdigitated channel is proposed. Computational fluid dynamics (CFD)-based simulations are used to study the flow distribution of this new type flow field and the results show that the flow distribution is uneven. So, we propose an optimization model to eliminate flow maldistribution. Finally, an optimized slotted-
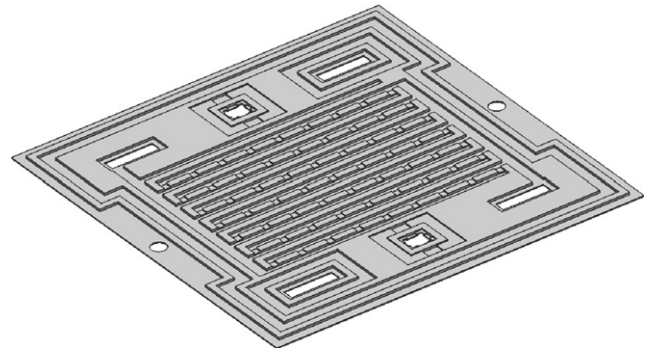

Fig. 2. Schematic diagram of slotted-interdigitated channel.

interdigitated channel is given to obtain an evenly distributed flow field.

2. Slotted-interdigitated channel

In order to reduce the pressure drop of interdigitated flow channel, small slots are designed at the reactant flow field side in the present study. Fig. 2 shows a schematic diagram of slotted-interdigitated channel with uniformly distributed slots on the rib of reactant flow field. As shown, the depth of the slot is smaller than the height of the rib to make sure that a continuous cooling channel is provided at the opposite side of the bipolar plate. A schematic diagram of the opposite side of slotted-interdigitated channel, which shows a continuous serpentine channel is shown in Fig. 3.

Computational fluid dynamics (CFD)-based simulation is used to study the flow distribution of this new type of flow field. The flow distribution of the slotted-interdigitated channel (Fig. 2) is studied using the commercial CFD code CFD-ACE+ developed by CFD Research Corporation. Fig. 4 shows the calculated results. As shown, an uneven distributed flow field which has slow velocity in the center part of the field is observed.
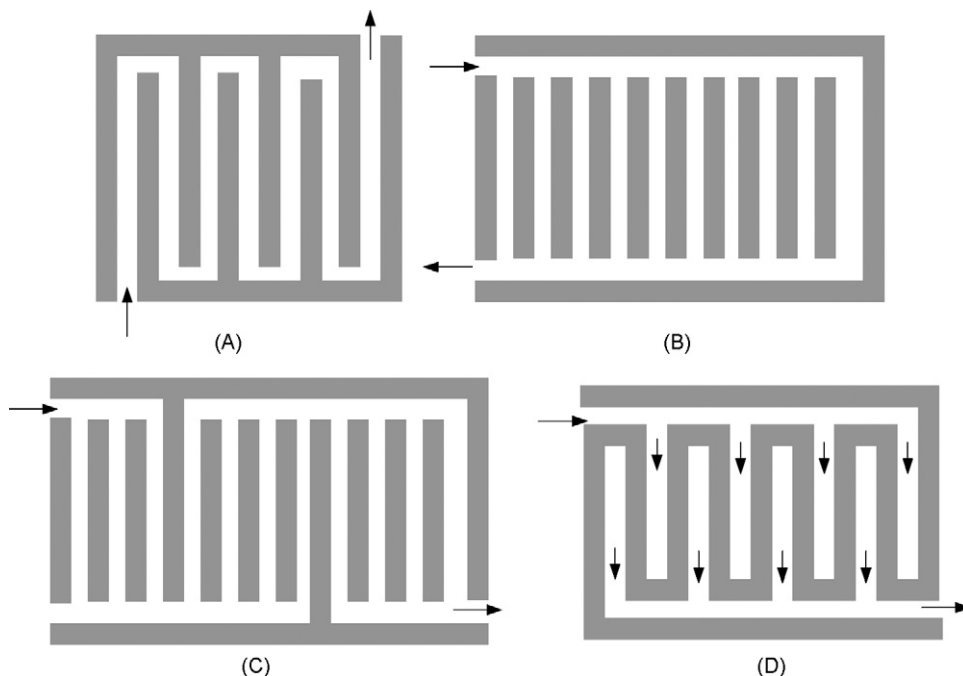

Fig. 1. Schematic diagram of (A) serpentine; (B) parallel; (C) discontinuous; (D) interdigitated type channel configurations.
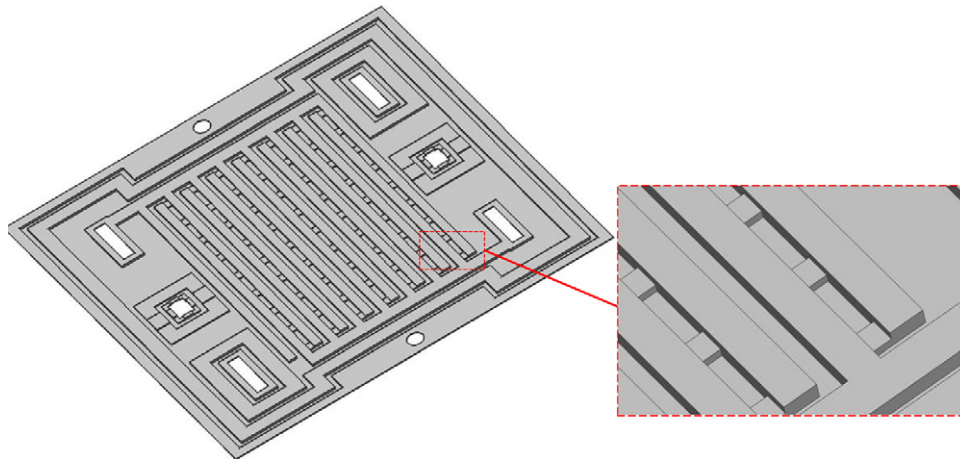
Fig. 3. Schematic diagram of the opposite side of slotted-interdigitated channel.
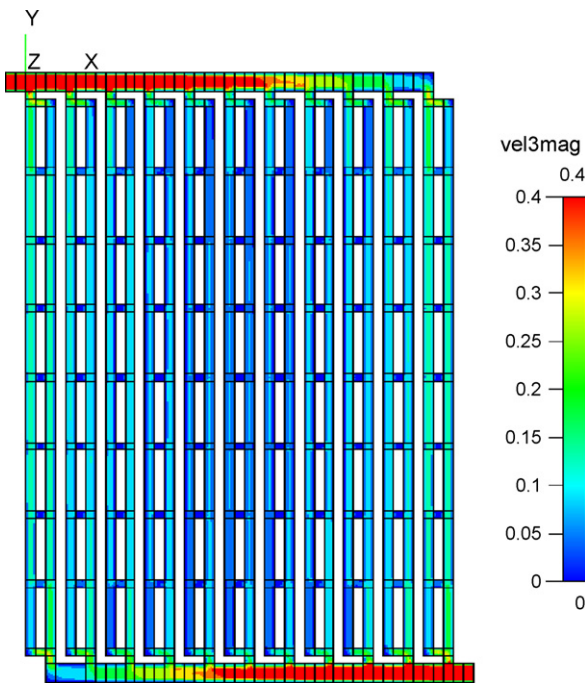

Fig. 4. Flow distribution of the slotted-interdigitated channel.

After careful analyses of the modeling results, we found that this uneven flow field is likely attributed to the following reasons:

1. The dividing and combining flow. Consider two neighboring channels connected by the slots (Fig. 5). V_0 is the inlet velocity. If no recirculation and back flow occurs at the corner (e.g., at the first corner), V_0 can be divided into two parts: V_1 and V_1' (V_1 is smaller than V_0). Similarly, $V_1 > V_2 > V_3 > V_4 > V_5 > V_6 > V_7 > V_8$, and resulting in an unevenly distributed flow field. In this study, we use only two slots laying at the inlet and outlet of two neighboring channels (Fig. 6) to avoid dividing and combining flow.
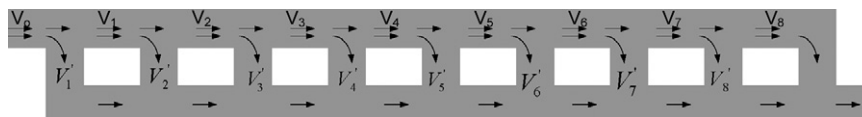
2. The other reason causing maldistribution is the property of parallel channels. The slotted-interdigitated channel can also been considered as another kind of parallel channel. The flow field shown in Fig. 4 is also an 11-channel Z-type parallel configuration. Parallel-channel configurations for PEMFC reduce the pressure drop, but may suffer from severe flow maldistribution. This aspect has been observed by other researches [14–15]. As shown in Fig. 4, higher flow speed exists at lateral channels and lower flow speed exists at central channels. To fix this problem, the dimensions of slots need to be optimized.

Two approaches are often used to analyze the flow distribution of bipolar plates: (i) CFD simulation, and (ii) analytical method. With the development of computer technology, CFD simulation are usually more versatile than analytical method, but CFD simulation cost more time and money. Because of the complexity of CFD code, it is also hard to optimize the geometric parameters of the bipolar plates to fix the flow maldistribution of parallel channels. In view of this, we adapt an analytical approach to optimize the dimensions of the slots. An analytical model is introduced first.

3. Model description

3.1. Assumptions

The model is set up based on the following assumptions:

1. The analysis here assumes the flow properties (e.g., the mass density, the viscosity) are constant.
2. The Reynolds numbers are low, the flow is considered as a laminar flow and the temperature is nearly uniform.
3. The dividing and the combining losses of pressure are neglected in comparison with the straight channel because of the low Reynolds number and the high length-to-diameter ratio of the channel [15].
4. The reactant gas is considered to flow in impervious channels. It does not consider the mass flow between the reactant channel and electrolyte. This may be a significant assumption, but it is necessary for simplifying the model [16].
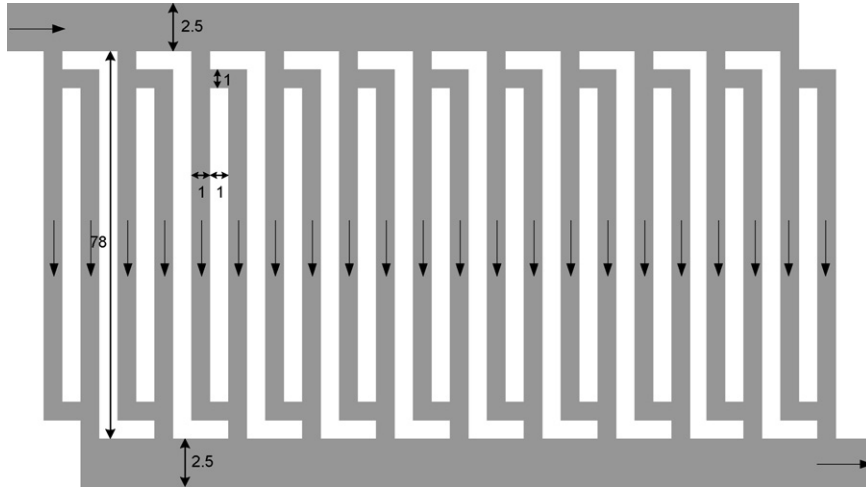

Fig. 5. Schematic diagram of two neighboring channels.

Fig. 6. Schematic diagram of slot design (units: mm).

3.2. Hagen–Poiseuille flow

For a straight channel, steady Hagen–Poiseuille flow, pressure drop, shown in Eq. (1), is needed to balance shear stress caused by the walls.

$$(p_{in} - p_{out})A_c = \tau_w P_c L_c \tag{1}$$

where P_{in} and P_{out} are the pressure of the inlet and outlet of the channel, respectively. A_c is cross-sectional area of the channel. P_c is the cross-sectional perimeter of the channel, and L_c is the channel length.

The shear stress can be represented by using friction factor f as follows:

$$f = \frac{\tau_w}{1/2 \rho \bar{v}^2} \tag{2}$$

where $\bar{v}$ is the mean velocity of the channel. Here, f is the friction factor given by the empirical correlation of Kays and Crawford [17]:

$$Re f = 13.84 + 10.38 \exp\left(\frac{-3.4}{\alpha}\right) \tag{3}$$

where $\alpha = w_c/b_c$ is the channel aspect ratio. And Reynolds number is

$$Re = \frac{\rho \bar{v} D_c}{\mu} \tag{4}$$

where D_c is the hydraulic diameter $D_c = 4W_c b_c/2(W_c + b_c)$.

From Eq. (1)–(4), we get

$$\Delta p = p_{in} - p_{out} = \frac{1}{2} \frac{(Re\, f)\mu P_c L_c}{D_c A_c} \bar{v} = R \bar{v} \tag{5}$$

where

$$R = \frac{1}{2} \frac{(Re\, f)\mu P_c L_c}{D_c A_c} \tag{6}$$

R can be considered as the fluidic resistance of the channel. Eq. (5) tells us that for a straight channel with geometric dimensions given, the pressure drop is proportional to the mean velocity because the fluidic resistance of channel is constant.

3.3. Analytical model for slotted-interdigitated channel

The flow distribution of slotted-interdigitated channel, with the flow velocity of the inlet header given, will be discussed to predict the mean velocity through each of the channels. In order to get velocity distribution of a slotted-interdigitated configuration with n channels, a configuration with 3 channels will be discussed first.

3.3.1. Model for a 3-channel plate

Consider a slotted-interdigitated configuration with 3 channels shown in Fig. 7A. The flow field is discretized first (Fig. 7B), and the analytical model is set up based on solving the pressure and mass balance equations. This model assumes that the cross-sectional area of the inlet header, which is represented by A_h, is uniform and is equal to that of the outlet header.

As shown in Fig. 7(B), P_i is the pressure at dividing or combing points, V_i and v_i present the mean velocity of channel, R_i and r_i are the resistance of channel. A_i and a_i present the cross-sectional area of channel in consistent with V_i and v_i.

According to the pressure balance,

$$V_{12}R_{12} + V_2 R_2 + v_{21}r_{21} + v_{23}r_{23} + V_2 R_2$$
$$= V_1 R_1 + v_{11}r_{11} + v_{13}r_{13} + V_1 R_1 + V_{12'}R_{12'} \tag{7}$$

$$V_{23}R_{23} + V_3 R_3 + v_{31}r_{31} + v_{33}r_{33} + V_3 R_3$$
$$= V_2 R_2 + v_{21}r_{21} + v_{23}r_{23} + V_2 R_2 + V_{23'}R_{23'} \tag{8}$$

$$v_{11}r_{11} + v_{13}r_{13} = v_{12}r_{12} + v_{14}r_{14} \tag{9}$$

$$v_{21}r_{21} + v_{23}r_{23} = v_{22}r_{22} + v_{24}r_{24} \tag{10}$$

$$v_{31}r_{31} + v_{33}r_{33} = v_{32}r_{32} + v_{34}r_{34} \tag{11}$$

According to the mass balance,

$$V_{in}A_h = V_{12}A_h + V_1 A_1 \tag{12}$$

$$V_1 A_1 = v_{11}a_{11} + v_{12}a_{12} \tag{13}$$

$$v_{11}a_{11} = v_{13}a_{13} \tag{14}$$

$$v_{12}a_{12} = v_{14}a_{14} \tag{15}$$

$$V_{12}A_h = V_{23}A_h + V_2 A_2 \tag{16}$$

$$V_2 A_2 = v_{21}a_{21} + v_{22}a_{22} \tag{17}$$

$$v_{21}a_{21} = v_{23}a_{23} \tag{18}$$

$$v_{22}a_{22} = v_{24}a_{24} \tag{19}$$

$$V_{23}A_h = V_3 A_3 \tag{20}$$

$$V_3 A_3 = v_{31}a_{31} + v_{32}a_{32} \tag{21}$$

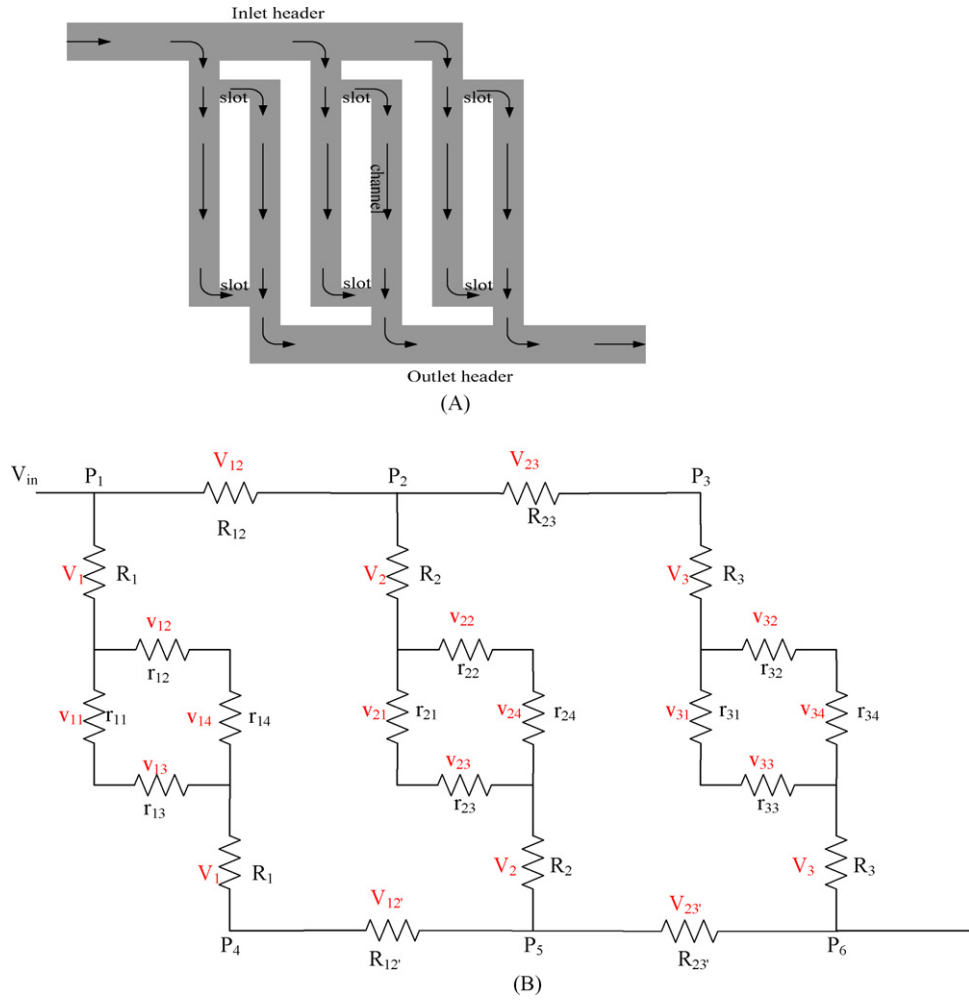$$v_{31}a_{31} = v_{33}a_{33} \tag{22}$$

Fig. 7. Schematic diagram of (A) Z-type configuration and (B) discrete channel model.

$$v_{32}a_{32} = v_{34}a_{34} \tag{23}$$

$$V_{12} + V_{12'} = V_{in} \tag{24}$$

$$V_{23} + V_{23'} = V_{in} \tag{25}$$

Combining Eq. (7)–(25), a linear matrix equation is derived,

$$M_{(3)} = R_{(3)}V_{(3)} \tag{26}$$

Eq. (26) implicitly shows that there are 19 unknowns for a slotted-interdigitated configuration with 3 channels, V_1, V_2, V_3, V_{12}, V_{23}, $V_{12'}$, $V_{23'}$, v_{11}, v_{12}, v_{13}, v_{14}, v_{21}, v_{22}, v_{23}, v_{24}, v_{31}, v_{32}, v_{33}, v_{34}. In matrix Eq. (26), and there are also 19 equations, r_i and R_i is known according to Eq. (6), if we know the inlet velocity V_{in}, then, we can solve the matrix equation to get the mean velocity at each channel.

3.3.2. Model for an n-channel plate

Similarly, we now consider a slotted-interdigitated configuration with n channels. The schematic diagram of the continuous channel and discrete channel model is shown in Fig. 8.

Like the method mentioned in Section 3.3.1, a matrix equation similar to Eq. (26) can be derived.

$$M_{(n)} = R_{(n)}V_{(n)} \tag{27}$$

The dimension of resistance matrix R is expanded from 19×19 to $(7n-2) \times (7n-2)$.

There are $7n-2$ unknowns in Eq. (27) and $7n-2$ equations; so we can solve the equations to get the velocity of each channel.

4. Optimization design

The model proposed in Section 3 is used to obtain a uniform flow distribution. It is possible to have a uniform flow distribution in the slotted-interdigitated channels by having a very large header cross-sectional area compared with that of a channel. Unfortunately, this will decrease the active geometrical area of the bipolar plate. A uniform flow distribution in the slotted-interdigitated channels can also be obtained by changing the cross-sectional area of the slots, increasing the cross-sectional area of the slots in central channels which has low velocity, decreasing the cross-sectional area of the slots in lateral channels which has high velocity.

High-performance language MATLAB is used to optimize the flow distribution. The original geometric parameters of the plate have been shown in Fig. 6. The original height of channel and slot (not shown in Fig. 6) are 0.5 mm and 0.2 mm, respectively. The variables, object function and constraints are discussed below.

4.1. Variables

Here, the geometric dimensions of the plate are treated as constant parameters except the width and depth of each slot, which are represented by $w(i)$ and $d(i)$, respectively. The two slots laying at the inlet and outlet of two neighboring channels have the same geometric dimensions. For an 11-channel plate shown in Fig. 6, there are 22 variables: $w(1)$, $w(2)$, ..., $w(10)$, $w(11)$ and $d(1)$, $d(2)$, ..., $d(10)$, $d(11)$.
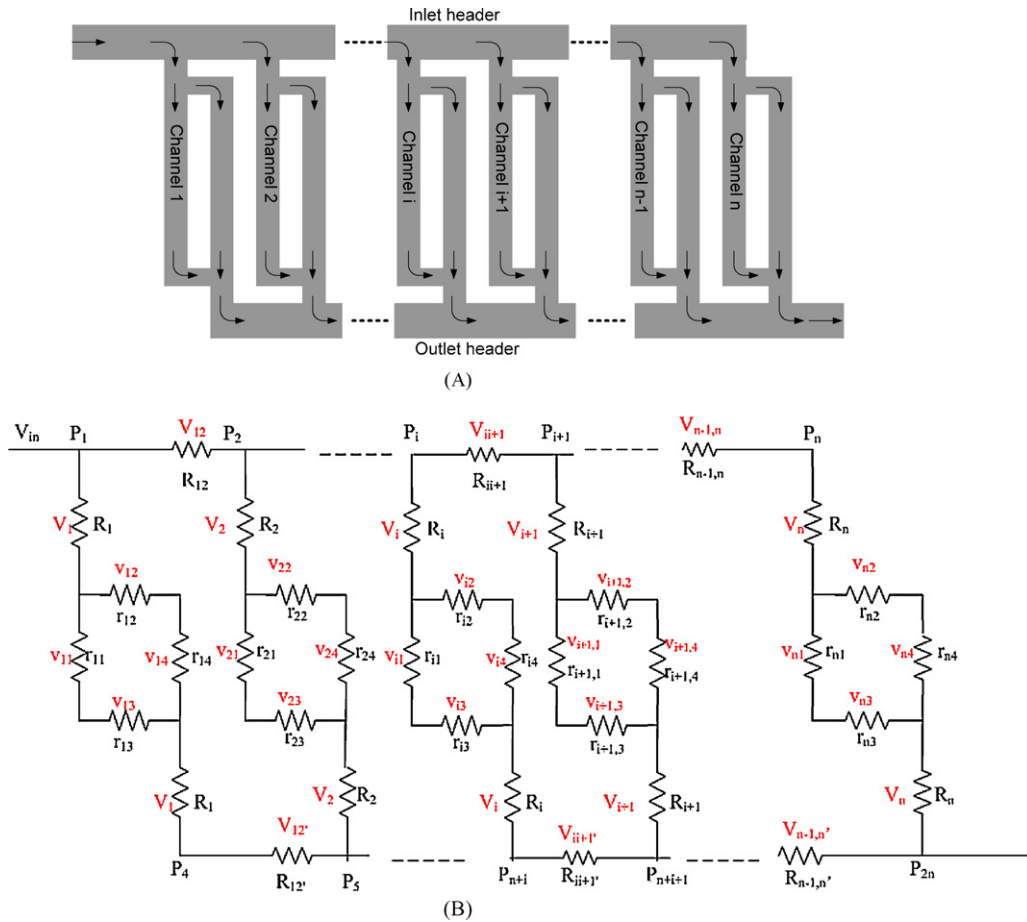
Fig. 8. Schematic diagram of (A) Z-type configuration and (B) discrete channel model.

4.2. Object function

Non-uniformity index, F, defined as [14,15]:

$$F = \frac{\sqrt{\sum_{i=1}^{n}(v_i - \bar{v})^2}}{n\bar{v}} \tag{28}$$

characterizing the relative flow split is treated as object function. Where v_i is a function of w_i and d_i

$$v_i = f(w(i), d(i)) \tag{29}$$

For an 11-channel plate, F becomes:

$$F = \frac{\sqrt{\sum_{i=1}^{11}(v_i - \bar{v})^2}}{11\bar{v}} \tag{30}$$

Here, F represents the non-uniformity of the flow distribution. If F equals to zero, all channels have the same flow velocity. The goal of this section is to minimize F by changing the variables.

4.3. Constraints

As mentioned above, in order to obtain a uniformly distributed flow field, we should increase the cross-sectional area of the slots in the center of the plate, and decrease the cross-sectional area of the slots near the inlet and outlet. For engineering purpose, bipolar plates should be symmetric, and we hope the slot width is in the range of 1–5 mm and slot depth is in the range of 0.1–0.3 mm. So,

the constraints are:

$$w(1) = w(11), w(2) = w(10), \ldots w(5) = w(7)$$
$$d(1) = d(11), d(2) = d(10), \ldots d(5) = d(7)$$
$$1 < w(i) < 5 \tag{31}$$
$$0.1 < d(i) < 0.3$$

4.4. Results and discussion

The commercial software MATLAB is used to optimize the flow field, and the optimized results are listed in Table 1 and Table 2.

In this case, the object function has a value of 4.6994e−008 according to the analytical model. Table 1 shows the widths of the slots. The minimum width is 1.001 mm, and the maximum one is 1.132 mm. These results indicate that the flow distribution is insen-

Table 1
Widths of the slots (units: mm).

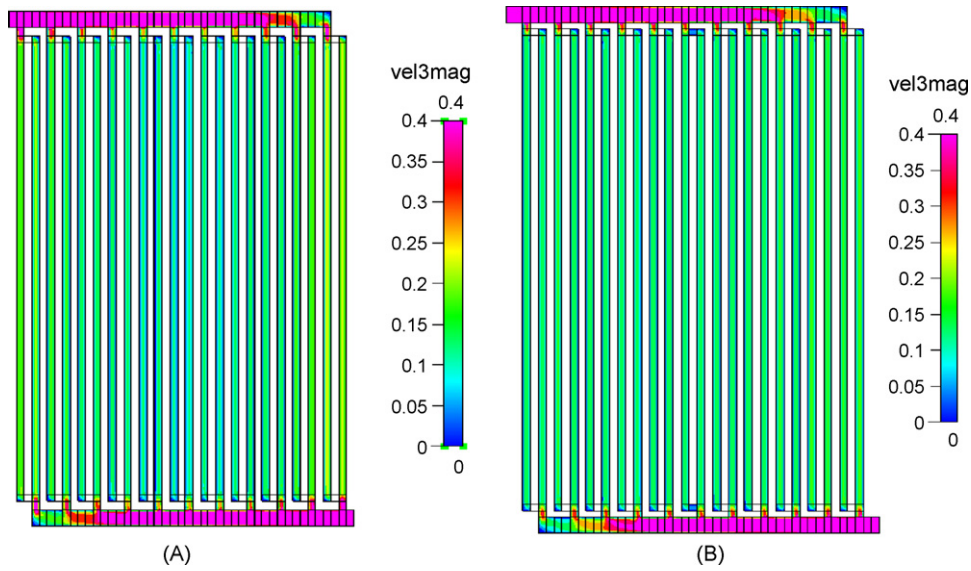|	
1	1.001
2	1.002
3	1.027
4	1.064
5	1.091
6	1.132
7	1.091
8	1.064
9	1.027
10	1.002
11	1.001

Fig. 9. Comparison of the contour results from CFD simulation. (A) Before optimization and (B) after optimization.

Table 2
Depths of the slots (units: mm).

1	0.112
2	0.129
3	0.153
4	0.190
5	0.250
6	0.296
7	0.250
8	0.190
9	0.153
10	0.129
11	0.112

Fig. 10. Comparison of the results from CFD and analytical model after optimization.

sitive to the width of the slot. Table 2 shows the depths of the slots. As shown, the depths changes from 0.112 mm to 0.296 mm.

Since the optimized result is insensitive to the width of the slot, to simplify the design process the width of the slot is considered as the constant parameter. Then, the number of variables changes from 22 to 11. They are the depths of the slots: $d(1),d(2),\ldots,d(10),d(11)$.

The widths of all slots are considered to be 1, the only variable is the depth of slot, and new optimization results are shown in Table 3.

In this case, the object function has a value of $1.0957e{-}007$ according to the analytical model.

The accuracy of the optimization results is verified by comparing the results of three-dimensional CFD simulations.

Fig. 9 shows comparison of the contour results from CFD simulation before and after optimization. As shown, the flow distribution of the optimized plate becomes more uniform than the original one. In order to quantitatively compare the flow distribution before and after optimization, the mean velocity at each joint face connecting

Table 3
Depths of the slots (units: mm).

1	0.105
2	0.121
3	0.144
4	0.182
5	0.243
6	0.298
7	0.243
8	0.182
9	0.144
10	0.121
11	0.105

inlet header and parallel channels is extracted from Fig. 9 and the results are shown in Fig. 10.

5. Conclusion

A new type of flow configuration, slotted-interdigitated channel, is proposed in the present study. However, CFD simulation results show that an arbitrary design of the slots causes severe flow maldistribution which comes from two aspects: (i) dividing and combining flow and (ii) the property of parallel channel.

To resolve problems above, the number of slots is decreased to two of each two neighboring channels and an analytical model, which is analogous to electric network, is presented to evaluate the flow distribution of the slotted-interdigitated channel. Furthermore, the analytical model proposed here is validated by comparison with results obtained from CFD simulations.

Finally, the model is used to optimize the dimensions of the plate, and a more uniformly distributed flow field is obtained.

Acknowledgements

References

[1] X. Li, I. Sabir, Int. J. Hydrogen Energy 30 (2005) 359–371.
[2] V. Mehta, J.S. Cooper, J. Power Sources 114 (2003) 32–53.
[3] A. Hermanna, T. Chaudhuria, P. Spagnol, Int. J. Hydrogen Energy 30 (2005) 1297–1302.
[4] N.G. Vitale, US Patent No. 5,981,098, 1999.
[5] J.K. Neutzler, US Patent No. 5,776,624, 1998.
[6] J.A. Rock, US Patent No. 6,503,653, 2003.
[7] L.G. Marianowski, US Patent No. 6,261,710, 2001.
[8] K.B. Shyam Prasad, S. Maharudrayya, S. Jayanti, J. Power Sources 159 (2006) 595–604.
[9] T.V. Nguyen, J. Electrochem. Soc. 143 (1996) 103–105.
[10] D.L. Wood III, J.S. Yi, T.V. Nguyen, Electrochim. Acta 43 (1998) 3795–3809.
[11] W. He, J.S. Yi, T.V. Nguyen, AIChE J. 46 (2000) 2053–2064.
[12] L. Wang, H. Liu, J. Power Sources 134 (2004) 185–196.
[13] G. Hu, J. Fan, S. Chen, Y. Liu, K. Cen, J. Power Sources 136 (2004) 1–9.
[14] R.J. Kee, P. Korada, K. Walters, M. Pavol, J. Power Sources 109 (2002) 148–159.
[15] S. Maharudrayya, S. Jayanti, A.P. Deshpande, J. Power Sources 144 (2005) 94–106.
[16] D. Martin, D.M. Guinea, B. Moreno, L. Gonzalez, M.C. Garcia-Alegre, D. Guinea, Int. J. Hydrogen Energy 32 (2007) 1572–1581.
[17] M. Kays,.E. Crawford, Convective Heat and Mass Transfer, McGraw-Hill, New York, 1980.